Marine Chemistry 252 (2023) 104248

Contents lists available at ScienceDirect

Marine Chemistry

journal homepage: www.elsevier.com/locate/marchem

Spatial and temporal occurrence of preformed nitrate anomalies in the subtropical North Pacific and North Atlantic oceans

Adam J. Smyth [a,b,*], Robert T. Letscher [a,b]

[a] Department of Earth Sciences, University of New Hampshire, Durham, NH 03824, United States of America
[b] Ocean Process Analysis Laboratory, University of New Hampshire, Durham, NH 03824, United States of America

ARTICLE INFO

Keywords:
Prefromed Nitrate
Vertically migrating phytoplankton
Tranparent exopolymer particles
Biogeochemical Argo

ABSTRACT

Preformed nitrate ($PreNO_3$) was formulated to act as a conservative tracer of ocean circulation after accounting for the stoichiometry of marine biochemical reactions involving oxygen and nitrate. However, $PreNO_3$ anomalies (e.g. negative values) have been identified within the shallow subsurface of the subtropical ocean which still have yet to be fully explained. The mechanisms proposed to drive the formation of $PreNO_3$ anomalies include: vertical export and remineralization of N-poor dissolved organic matter (DOM) or transparent exopolymer particles (TEP), and the actions of vertically migrating phytoplankton. In this study we use observations from the subtropical Pacific and Atlantic Oceans taken by twenty Biogeochemical Argo profiling floats to assess the spatiotemporal variability of negative subsurface and positive euphotic zone $PreNO_3$ anomalies and their formation rates. After explicitly accounting for the magnitude of DOM cycling, residual euphotic zone positive $PreNO_3$ anomalies and subsurface negative $PreNO_3$ anomalies are consistently observed between 40°S and 40°N. The seasonal timing of euphotic zone positive residual $PreNO_3$ anomaly formation in relation to subsurface negative residual $PreNO_3$ anomalies suggests that both vertically migrating phytoplankton and the remineralization of N-deficient TEP likely contribute to the formation of residual $PreNO_3$ anomalies, but with regional variance suggesting a potentially larger role for migrating phytoplankton in the North Pacific and TEP processes in the North Atlantic. Since migrators include large diatoms that produce ballasted organic matter while TEP may only sink shallowly before remineralization, further investigation into the mechanisms generating $PreNO_3$ anomalies and their quantitative significance is needed to assess the future trajectory of the biological carbon pump in an expanding subtropical ocean ecosystem.

1. Introduction

Preformed nitrate ($PreNO_3$), also known as 'NO' (Broecker, 1974), is a theoretically conservative tracer derived from the residual in observed nitrate after accounting for the stoichiometry of oxygen and nitrate in marine biological reactions (Emerson and Hayward, 1995; Abell et al., 2005). $PreNO_3$ quantifies the amount of nitrate present in a water parcel when it leaves the surface and was originally derived to trace the mixing and circulation of deep water, since deep waters formed in different parts of the world ocean will have different characteristic $PreNO_3$ values (Broecker, 1974). The calculation of $PreNO_3$ utilizes the well-known Redfield ratio to account for the O_2:N stoichiometry of biological reactions such as photosynthesis and respiration (Redfield et al., 1963). As formulated, $PreNO_3$ should be positive everywhere below the euphotic zone. However significant $PreNO_3$ anomalies (e.g. negative values) have been identified within the shallow subsurface (~100–250 m) of the subtropical ocean including at the Hawaiian Ocean Time series (HOT) and the Bermuda Atlantic Time Series (BATS) sites, and elsewhere in the subtropical North Pacific (Emerson and Hayward, 1995; Johnson et al., 2010; Letscher and Villareal, 2018; Fawcett et al., 2018). In addition, positive $PreNO_3$ anomalies have been identified within the euphotic zone (< ~100 m) at the time series sites (Letscher and Villareal, 2018; Fawcett et al., 2018) and elsewhere across the subtropical North Pacific (Abell et al., 2005), a depth horizon that should carry a $PreNO_3$ value of zero given its strong influence from biogeochemical processes and remoteness from known water mass formation regions.

The presence of these anomalies reveal biogeochemical processes operating with non-Redfield O_2:N stoichiometries describing biological consumption or production of oxygen without stoichiometric nitrate production or consumption, respectively. The presence of $PreNO_3$

* Corresponding author at: Department of Earth Sciences, University of New Hampshire, Durham, NH 03824, United States of America.
E-mail address: ajsmyth17@gmail.com (A.J. Smyth).

https://doi.org/10.1016/j.marchem.2023.104248
Received 20 August 2022; Received in revised form 30 March 2023; Accepted 14 May 2023
Available online 25 May 2023
0304-4203/© 2023 Elsevier B.V. All rights reserved.

anomalies, of which the causative mechanisms have only been partially explained, highlight gaps in the current understanding of the stoichiometry governing the linked marine biogeochemical cycles of nitrogen, oxygen, and carbon in the ocean. The nitrogen and carbon cycles are tightly coupled on seasonal to millennial timescales (Gruber, 2008), making filling the gaps in our understanding of the nitrogen cycle important as scientists work to study the ocean biogeochemistry feebacks with the changing 21st century climate as a result of anthropogenic perturbation. The subtropical ocean ecosystem is predicted to expand as a result of changes in climate (Polovina et al., 2011), which may result in the mechanism(s) driving the formation of subtropical $PreNO_3$ anomalies to play a greater role in ocean biogeochemistry into the future.

Changes in dissolved nutrients and gases are linked by the stoichiometry of biochemical reactions. The stoichiometry of marine biochemical reactions is thought to follow the canonical Redfield Ratio, 106C: 16 N: 1P: −138 O_2 (Redfield et al., 1963). Negative $PreNO_3$ anomalies can form when there is biological oxygen consumption without (Redfieldian) stoichiometric nitrate production. Positive $PreNO_3$ anomalies can form when there is oxygen production without the corresponding amount of in situ nitrate consumption. To date, three mechanisms have been proposed that operate with non-Redfield stoichiometry to explain the formation of $PreNO_3$ anomalies: the export and sub euphotic zone remineralization of N-deficient DOM (Emerson and Hayward, 1995; Abell et al., 2005) or N-deficient transparent exopolymer particles (TEP; also known as gel-like organic matter; Fawcett et al., 2018), and vertically migrating phytoplankton (VMP) that can access sub euphotic zone stocks of nitrate, returning to photosynthesize in the euphotic zone above (Villareal et al., 2014).

Subsurface negative $PreNO_3$anomalies were first observed in the subtropical North Pacific by Emerson and Hayward (1995) where it was suggested that their occurrence could be explained by the export and remineralization of N-poor DOM. This suggestion was later supported by the findings of Abell et al. (2005), where observations from the subtropical North Pacific for the magnitude of DOM remineralization and its non-Redfield, N-poor stoichiometry largely removed any subsurface negative anomalies for their calculations of $PreNO_3$. Then in 2010, Johnson et al., using one of the first BGC-Argo profiling floats equipped with both nitrate and oxygen sensors deployed near Station ALOHA in the subtropical North Pacific, observed the seasonal occurrence of negative $PreNO_3$ anomalies below the 1% light level. These authors attempted to link the summertime drawdown of dissolved inorganic carbon (DIC) in the surface mixed layer without the presence of sufficient amounts of nitrate to the observed subsurface negative $PreNO_3$anomalies (Johnson et al., 2010). It was suggested that $PreNO_3$ anomaly formation could be caused by a dual physical and biological mechanism whereby synoptic vertical physical transport events at the base of the euphotic zone inject nitrate into the lower euphotic zone followed by VMP consuming this nitrate and then returning to the mixed layer to photosynthesize. VMP was suggested because the missing nitrate could not be moved by a fully physical mechanism because physical transport would also bring DIC to the surface, erasing the observed summertime DIC drawdown (Johnson et al., 2010).

More recently, the export and subsurface remineralization of carbon-rich, gel-like organic matter particles (also known as TEP) have been suggested to be a previously overlooked mechanism that could drive the observed vertical patterns of $PreNO_3$ anomalies (Fawcett et al., 2018). TEP are abiotically formed from the coagulation of carbohydrates with a high carbon to nitrogen ratio (>20:1; Engel and Passow, 2001; Mari et al., 2017) that are produced by phytoplankton and aggregate to form gel-like particles (Alldredge et al., 1993; Wurl et al., 2011; Mari et al., 2017). TEP is initially positively buoyant upon formation, but as TEP aggregates or becomes ballasted at the surface it eventually becomes negatively buoyant causing TEP to sink out of the euphotic zone (Wurl et al., 2011; Mari et al., 2017; Fawcett et al., 2018). Vertical profiles of TEP show elevated concentrations closer to the surface with a decrease with depth similar to other known marine organic matter pools (Engel, 2003; Wurl et al., 2011; Cisternas-Novoa et al., 2015). This vertical distribution is consistent with a mechanism to explain euphotic zone positive and subsurface negative $PreNO_3$ anomalies (Fig. 1a), given TEP's N-deficient stoichiometry. TEP sinks slowly, on the order of ~10's meters per year (Mari et al., 2017). Thus any TEP contribution to $PreNO_3$ anomaly formation should exhibit a 'lagged' upper ocean/subsurface timing, with positive $PreNO_3$ anomalies observed within the euphotic zone leading subsurface negative $PreNO_3$ anomaly formation by weeks to months to allow for significant TEP formation, export, and remineralization. The extent to which bacteria degrade TEP is still not well understood and may include concomitant inorganic N consumption, requiring further investigation (Busch et al., 2017; Fawcett et al., 2018). Nutrient limitation is thought to stimulate the production of TEP, which could describe why TEP is more prevalent in the subtropical ocean (Myklestad, 1995; Mari et al., 2017).

The third suggested mechanism to explain the formation of upper ocean $PreNO_3$ anomalies involves vertically migrating phytoplankton (VMP), which can consume nitrate at depth within the nitracline and return towards the surface producing oxygen as they photosynthesize (Fig. 1b; Villareal et al., 2014). This pattern can generate positive $PreNO_3$ anomalies within the euphotic zone as photosynthetic oxygen evolution occurs in a layer where nitrate is not being consumed and negative $PreNO_3$ anomalies can form within the shallow nitracline where vertical migrators consume nitrate generated via the respiration of exported organic matter, disrupting the Redfieldian accumulation of nitrate. Examples of phytoplankton taxa with documented vertical migrating behavior include: *Pyrocystis* a dinoflagellate (Sukhanova and Rudyakov, 1973; Ballek and Swift, 1986; Rivkin et al., 1984), *Ethmodiscus* a diatom (Villareal and Lipschultz, 1995; Villareal et al., 1999), and *Rhizosolenia* a 'mat' forming diatom (Villareal and Carpenter, 1994; Pilskaln et al., 2005; Villareal et al., 2014). Migratory behavior is achieved via buoyancy regulation which may be mediated by light cues and/or internal nitrate stores (Villareal et al., 1996). The whole migratory cycle of VMP taxa has been estimated to take 4–5 days (Villareal et al., 1996). Therefore evidence for VMP contributing to $PreNO_3$ anomaly formation should exhibit contemporaneous positive anomalies within the euphotic zone and negative anomalies immediately below within the nitracline.

Letscher and Villareal (2018) formulated a new calculation of $PreNO_3$, termed residual $PreNO_3$, that specifically accounts for the fractions of oxygen use attributed to sinking particulate organic matter (POM) and non-Redfield DOM (Eq. (1)). The use of the residual $PreNO_3$ calculation aids in the identification of positive and negative $PreNO_3$ anomalies by accounting for the non-Redfield stoichiometry of DOM or POM that is known to exist in the subtropical ocean (Martiny et al., 2013; Teng et al., 2014; DeVries and Deutsch, 2014; Letscher and Moore, 2015). It was determined that the non-Redfield cycling of DOM and POM at the subtropical HOT and BATS time series sites could explain ~15–33% of the annually observed $PreNO_3$ anomalies, leaving significant unexplained residual $PreNO_3$ anomalies (Letscher and Villareal, 2018). Thus the occurrence of residual $PreNO_3$ anomalies identify the actions of the two remaining non-Redfield biogeochemical processes: TEP cycling and VMP. TEP cycling was estimated to contribute 5–7% of the observed $PreNO_3$ anomaly formation rate at BATS and 37–50% at HOT based on sparse measurements of TEP vertical profiles in the subtropical North Atlantic and Pacific Oceans with the remainder ascribed to the VMP mechanism. Fawcett et al. (2018) working at the BATS site in the North Atlantic provided stable isotopic evidence of nitrate consumption occurring within the layer directly below the euphotic zone, which they ascribe to uptake by heterotrophic bacteria in order to consume N-poor TEP. However another plausible explanation for the nitrate isotope data at BATS is to ascribe the uptake of nitracline nitrate to migrating autotrophs. Thus, the studies of Letscher and Villareal (2018) and Fawcett et al. (2018) reach opposing conclusions for the most likely mechanism responsible for residual $PreNO_3$(anomalies)

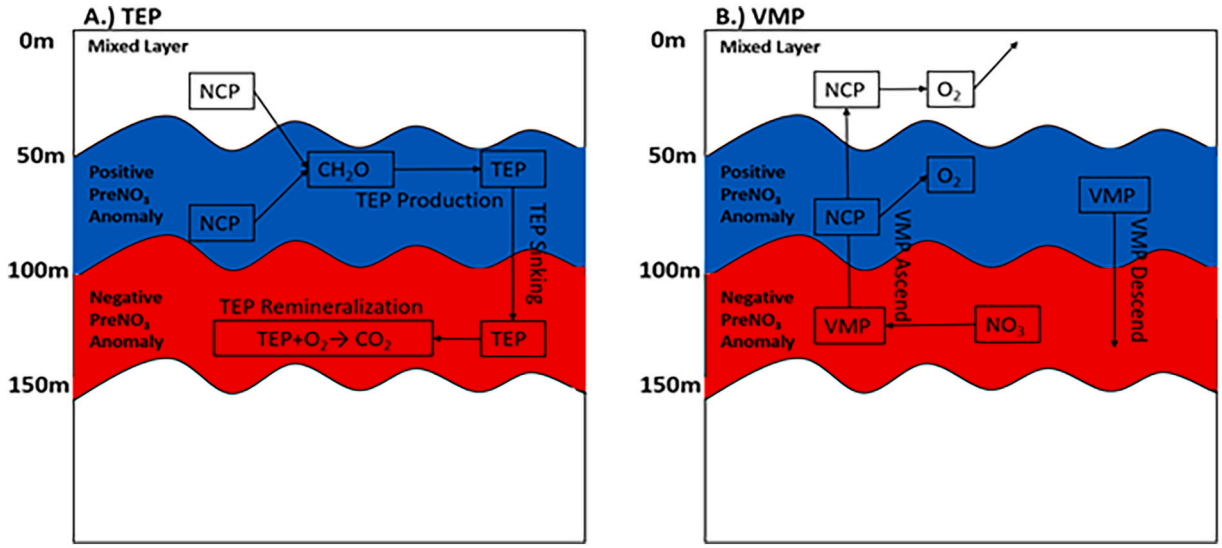

Fig. 1. Mechanisms of euphotic zone positive $PreNO_3$ anomaly and sub-euphotic zone negative $PreNO_3$ anomaly formation. A.) TEP mechanism depicting production of N-deficient carbohydrates (CH_2O) as a result of net community production (NCP), generating a positive $PreNO_3$ anomaly within the euphotic zone (0–100 m). CH_2O abiotically forms TEP which slowly sink below 100 m to be remineralized using O_2, generating a negative $PreNO_3$ anomaly within 100–150 m. B.) VMP mechanism depicting VMP descent below 100 m to acquire NO_3 without in situ photosynthesis, generating a negative $PreNO_3$ anomaly within 100–150 m. Upon ascent above 100 m, NCP driven in part by VMP evolves O_2 using nitracline NO_3, generating a positive $PreNO_3$ anomaly.

In this study, we investigate the potential mechanisms that lead to $PreNO_3$ anomalies by seeking the answers to the following two questions:

1.) What is the seasonality, geographic extent, and rates of subsurface negative $PreNO_3$ anomalies and euphotic zone positive $PreNO_3$ anomalies in the global subtropical ocean?
2.) What biogeochemical processes capable of generating $PreNO_3$ anomalies are consistent with the timing and vertical distribution of anomaly generating events observed in the BGC-Argo float records?

We sought the answers to both of these questions by looking at spatiotemporal patterns in the occurrence of $PreNO_3$ anomalies as well as the rates at which $PreNO_3$ anomalies form within the dissolved nitrate and oxygen records of BGC-Argo floats transiting the subtropical ocean. Once BGC-Argo floats are deployed they start a ten-day cycle starting with an initial decent to a parking depth of 1000 m where they remain for roughly nine and a half days. The BGC-Argo float then descends deeper to 2000 m before ascending to collect vertically-resolved observations towards the surface where it transmits its data to satellite (Claustre et al., 2019). Our analysis investigates twenty BGC-Argo float records that transitted the tropical, subtropical, and subtropical to mid-latitude transistion regions of the ocean between 40°S and 40°N. This latitudinal range was selected based on prior knowledge of subsurface negative $PreNO_3$ anomaly extent as observed within the World Ocean Atlas nitrate and oxygen climatologies (see Fig. 2a). Based on these observations and prior studies it is hypothesized that $PreNO_3$ anomalies within the BGC-Argo record would be observed throughout the subtropical ocean with a seasonality for $PreNO_3$ anomaly generation that peaks during the summer months. We hypothesize that the float records would provide evidence for both the TEP cycling and VMP mechanisms to contribute to $PreNO_3$ anomaly formation with perhaps a regional preponderance for one over the other.

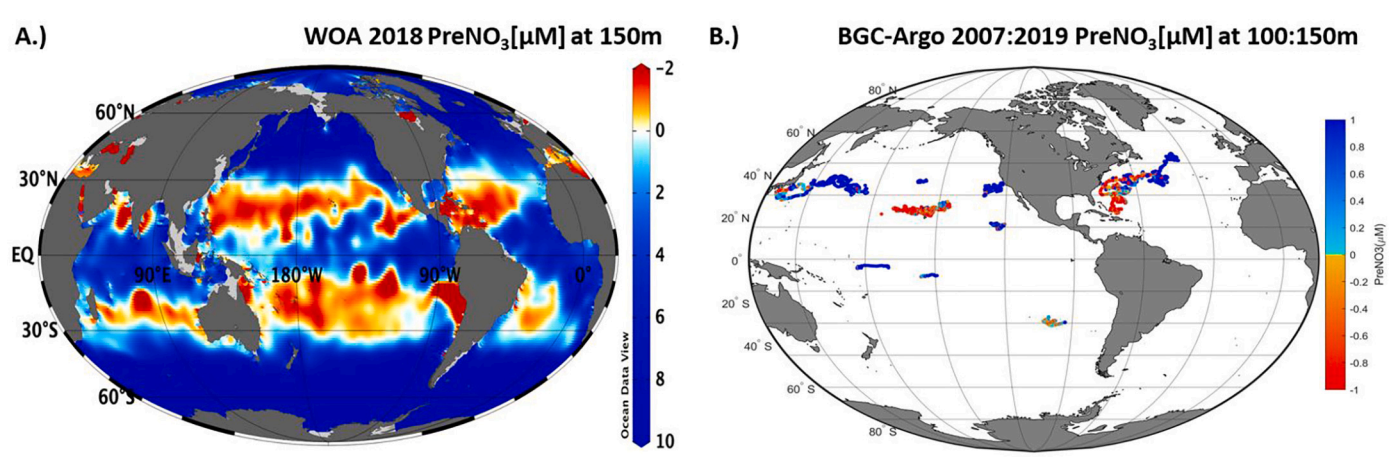

Fig. 2. A.) Annual mean residual $PreNO_3$ [μM] at 150 m calculated using median ocean basin and depth specific constants from Table 1 using dissolved oxygen and nitrate data from World Ocean Atlas 2018 (Garcia et al., 2018a, 2018b). B.) Residual $PreNO_3$ [μM] from 100 to 150 m along float paths of the 20 BGC-Argo floats from years 2007:2019. Residual $PreNO_3$ range limited to −1 to 1 μM to highlight negative (red) and positive (blue) values. (For interpretation of the references to colour in this figure legend, the reader is referred to the web version of this article.)

2. Materials and methods

2.1. Data access

Twenty Biogeochemical Argo profiling floats were selected that traversed between 40°N–40°S for retrieval of observed nitrate, salinity, potential density, temperature, oxygen, time, and position. The twenty floats were: Bermuda 6391, Bermuda 6975, Bermuda 6976, Bermuda 7663, Hawaii 5145, Hawaii 6401, Hawaii 6403, Hawaii 6891, Hawaii 8486, Hawaii 8497, CalCurrent 7647, CalCurrent 7618, Kuroshio 7546, Kuroshio 7674, EQPACW 8474, EQPACW 12788, ETNP 7558, ETNP 6960, NoPacific 7642, and SoPacific 7553. These twenty floats collected data primarily between 30°S and 50°N from 2007 to 2019. The mean length of the float records for these twenty floats was 3.15 years. This data was accessed throught the MBARI Floatviz 6.0 data portal (MBARI, 2017). All observations from these BGC-Argo floats have associated quality flags for: good, questionable, bad, or missing or not inspected (MBARI, 2017). Additionally there is a option to download either the raw or adjusted data (MBARI, 2017). Adjusted data with the data quality flag 'Good Only' was downloaded via the MBARI Floatviz website (http://www.mbari.org/science/upper-ocean-systems/chemical-sensor-group/floatviz/). Analyses of the float records were restricted to data that was collected in the upper 350 m.

2.2. PreNO$_3$ calculation

Values of PreNO$_3$ were calculated using the residual PreNO$_3$ formulation described in Letscher and Villareal (2018) including ocean-basin and depth-specific constants (Table 1):

$$\text{residual PreNO}_3 = \text{NO}_{3\text{meas}} - \frac{f_{POM} \bullet AOU}{r_{POM}} - \frac{f_{DOM} \bullet AOU}{r_{DOM.}} \quad (1)$$

f_{POM} and f_{DOM} is the fraction of oxygen use attributable to POM and DOM remineralization, respectively (Eq. (1); Letscher and Villareal, 2018). r_{POM} and r_{DOM} is the ratio of molecular oxygen used per mole of nitrogen for POM and DOM remineralization, respectively (Eq. (1); Letscher and Villareal, 2018). Apparent Oxygen Utilization (AOU) quantifies the oxygen saturation anomaly due to biological consumption or production of oxygen through respiration or photosynthesis, respectively, and was calculated using code written by Peltzer (2007).

PreNO$_3$ values were calculated using 27 different combinations of f_{DOM}, f_{POM}, r_{POM}, and r_{DOM} to capture the estimated uncertainty in each parameter, which is dependent on differences in depth, potential density, or ocean basin (Eq. (1); Table 1; Letscher and Villareal, 2018). Three discrete depth/density layers were investigated for further analysis: 25-75 m representing the euphotic zone immediately below the surface mixed layer as to ignore air-sea O_2 fluxes, and a shallower and deeper subsurface density layers that approximately bisected the observed thickness of the negative PreNO$_3$ anomalous layer. Note f_{DOM}, f_{POM}, r_{POM}, and r_{DOM} were estimated empirically from time-series data at Station ALOHA in the subtropical North Pacific and the BATS site in the subtropical North Atlantic (Table 1; Letscher and Villareal, 2018) and have been applied across the subtropical Pacific and Atlantic Oceans here. The values of r_{POM} represent the minimum, the Redfield ratio, and maximum estimates from the published literature (Table 1; Paulmier et al., 2009). Due to the differences in the values used to calculate residual PreNO$_3$ in the Pacific and the Atlantic, there is more variability between the 27 different calculations of residual PreNO$_3$ in the Atlantic then there is in the Pacific (Table 1). The 27 different calculations of residual PreNO$_3$ is meant to account for the uncertainty in applying empirically derived values for f_{DOM}, f_{POM}, and r_{DOM} determined at Station ALOHA and the BATS time series sites to the larger Pacific and Atlantic Ocean basins, respectively. The mean and variance of the 27 different calcuations of residual PreNO$_3$ are used for subsequent temporal analysis of anomaly formation rates.

2.3. Rates of PreNO$_3$ anomaly formation

To calculate the rates of residual PreNO$_3$anomaly formation (μmol N m^{-3} d^{-1}) within the three discrete depth/density layers within each individual float record, the mean of the 27 different calculations of residual PreNO$_3$ was smoothed by a running average with a non-stationary window size dependent on the number of observations that were taken each individual month. Ninety-five percent confidence intervals were calculated based on the standard error associated with averaging the 27 different values for residual PreNO$_3$as well as the standard error for smoothing the time series. Regressions were then calculated between local maxima and minima of residual PreNO$_3$ observations against time using the method of least squares. Local minima and maxima within the float records were identified for each year by using the Matlab™ function, *islocalmax*, with the absolute smoothed residual PreNO$_3$ values as the input (The MathWorks™, Inc, 2019). The input argument *MinSeparation* was used to specify the minimum distance between points that were identified as local maxima or minima (The MathWorks™, Inc, 2019). The argument *MaxNumExtrema* was used to set the maximum number of minima or maxima that would be identified for each year (The MathWorks™, Inc, 2019). The number of regressions for each time series as well as the length of the regressions were specified by using the combination of these input arguments. To avoid the introduction of any bias, a value of 20 was used for *MaxNumExtrema* (i.e. at most 20 minima or maxima would be identified) and a value of 2 was used for *MinSeparation* (i.e. at least a two month separation between identified minima or maxima) for all profiling floats to determine the rates of residual PreNO$_3$anomaly formation. These values were selected to identify seasonal-scale residual PreNO$_3$ anomaly formation events and to de-emphasize diel variability. The mean residual PreNO$_3$ concentration (μM) and its associated standard error was calculated by using the residual PreNO$_3$ concentrations in each depth/density layer (Table 2).

3. Results

3.1. Subtropical ocean residual PreNO$_3$ anomalies

Residual PreNO$_3$ derived from the World Ocean Atlas 2018 climatology at 150 m indicates that negative PreNO$_3$ anomalies occur primarily between 30°S and 30°N (Fig. 2A) and are absent within ~3–5° of the equator. Whereas positive PreNO$_3$ values are generally more prevelent poleward of 30°S and 30°N as well as within equatorial regions (Fig. 2A), reflecting the PreNO$_3$ concentrations present within subsurface water masses formed within the mid to high latitudes and the upwelling of these water masses near the equator. A similar spatial pattern can be seen in the residual PreNO$_3$ values derived within 100-150 m from the twenty BGC-Argo floats investigated in this study (Fig. 2B). BGC-Argo derived residual PreNO$_3$ within 100-150 m indicate that

Table 1
Constants for the calculation of residual PreNO$_3$ and how they were varied for different depths, isopycnals, and oceans. Values based on Letscher and Villareal (2018).

	Pacific				Atlantic			
	f_{DOM}	f_{POM}	r_{POM}	r_{DOM}	f_{DOM}	f_{POM}	r_{POM}	r_{DOM}
0-100 m or σ_θ:24.2–24.7	0.5 ± 0.1	0.5 ± 0.1	10.6, 8.75, or 6.9	18.1	0.4 ± 0.1	0.6 ± 0.1	10.6, 8.75, or 6.9	21.1
$\sigma_\theta > 24.7$	0.5 ± 0.1	0.5 ± 0.1	10.6, 8.75, or 6.9	18.9	0.4 ± 0.1	0.6 ± 0.1	10.6, 8.75, or 6.9	21.1

Table 2
Observed rates of positive and negative residual $PreNO_3$ anomaly formation for each individual Hawaii and Bermuda float. Mean locations (lat/lon), anomaly formation rates (μmol N m^{-3} d^{-1}), trend lengths (days), residual $PreNO_3$ [μM], and regression correlation (r^2), are reported for three depth/density layers: 25-75 m and two subeuphotic zone isopycnals layers. NA indicates that no positive or negative rates of anomaly formation were observed; ± is standard error.

Float Name	Layer	Mean Location	Mean Positive $PreNO_3$ Rate $\left(\frac{\mu mol\ N}{m^3\ day}\right)$	Mean Negative $PreNO_3$ Rate $\left(\frac{\mu mol\ N}{m^3\ day}\right)$	Mean Length of Positive Trends (days)	Mean Length of Negative Trends (days)	Mean $PreNO_3$ (μM)	Mean r^2
Hawaii 5145	25 m to 75 m	22.87°N,157.99°W	5.91 ± 2.04	-2.82 ± 0.77	84.80 ± 15.21	81.67 ± 9.64	0.04 ± 0.01	0.54 ± 0.12
	σ_θ = 24.5–24.9	22.87°N,157.99°W	2.55 ± 0.65	-3.53 ± 1.97	134.40 ± 31.01	70.00 ± 8.50	−0.49 ± 0.02	0.28 ± 0.08
	σ_θ = 24.9–25.3	22.87°N,157.99°W	0.96 ± 0.63	-2.12 ± 0.98	134.50 ± 47.50	145.75 ± 51.26	−0.54 ± 0.01	0.38 ± 0.12
Hawaii 6401	25 m to 75 m	22.69°N,157.99°W	4.30 ± 1.01	-5.68 ± 1.64	147.83 ± 21.57	106.00 ± 15.04	−0.01 ± 0.01	0.76 ± 0.09
	σ_θ = 24.25–24.75	22.69°N,157.99°W	2.19 ± 0.58	-3.76 ± 1.00	125.43 ± 16.55	103.80 ± 13.14	−0.92 ± 0.01	0.26 ± 0.07
	σ_θ = 24.75–25.25	22.69°N,157.99°W	1.34 ± 0.60	-1.33 ± 0.41	144.75 ± 19.90	80.67 ± 9.35	−0.67 ± 0.01	0.28 ± 0.08
Hawaii 6891	25 m to 75 m	22.68°N,157.99°W	1.68 ± 0.76	-3.65 ± 2.13	142.67 ± 25.64	61.33 ± 1.33	0.42 ± 0.01	0.29 ± 0.11
	σ_θ = 24.1–24.6	22.68°N,157.99°W	3.21 ± 2.41	-0.70 ± 0.26	121.33 ± 29.38	83.00 ± 22.01	−0.07 ± 0.03	0.25 ± 0.16
	σ_θ = 24.6–25.1	22.68°N,157.99°W	4.33 ± 0.96	-7.26 ± 0.75	115.25 ± 18.73	74.50 ± 16.50	−0.46 ± 0.02	0.62 ± 0.06
Hawaii 8497	25 m to 75 m	22.82°N,157.89°W	2.17 ± 0.88	-2.76 ± 0.92	151.00 ± 53.13	140.80 ± 24.78	0.16 ± 0.01	0.62 ± 0.12
	σ_θ = 24.2–24.75	22.82°N,157.89°W	3.32 ± 0.54	-2.53 ± 0.80	94.00 ± 17.62	111.22 ± 12.59	−0.29 ± 0.01	0.31 ± 0.09
	σ_θ = 24.75–25.3	22.82°N,157.89°W	2.50 ± 0.85	-1.23 ± 0.39	81.86 ± 9.17	118.00 ± 8.94	−0.29 ± 0.01	0.55 ± 0.10
Hawaii 8486	25 m to 75 m	22.68°N,158.04°W	4.88 ± 1.43	-5.26 ± 2.07	84.80 ± 11.08	101.33 ± 27.55	0.36 ± 0.01	0.67 ± 0.15
	σ_θ = 24.5–24.8	22.68°N,158.04°W	2.64 ± 0.98	-1.74 ± 1.02	113.50 ± 24.75	92.67 ± 17.61	−0.18 ± 0.02	0.31 ± 0.12
	σ_θ = 24.8–25	22.68°N,158.04°W	1.46 ± 0.94	-2.17 ± 0.42	135.00 ± 47.42	94.50 ± 29.50	−0.31 ± 0.02	0.21 ± 0.08
Hawaii 6403	25 m to 75 m	22.70°N,158.12°W	4.60 ± 1.19	-5.61 ± 0.90	187.40 ± 53.50	140.50 ± 5.50	0.21 ± 0.01	0.70 ± 0.12
	σ_θ = 24.3–24.8	22.70°N,158.12°W	4.94 ± 1.18	-3.00 ± 1.31	97.57 ± 13.46	180.00 ± 44.57	−0.22 ± 0.02	0.51 ± 0.09
	σ_θ = 24.8–25.2	22.71°N,158.12°W	2.72	-0.78 ± 0.31	154.00	173.71 ± 21.70	−0.63 ± 0.01	0.30 ± 0.13
Bermuda 6391	25 m to 75 m	31.74°N,64.32°W	6.69 ± 0.50	-4.29 ± 1.88	122.00 ± 29.00	136.75 ± 29.14	0.17 ± 0.01	0.76 ± 0.11
	σ_θ = 25.5–25.9	31.74°N,64.32°W	8.41 ± 3.60	-8.21 ± 4.93	195.67 ± 15.86	76.50 ± 6.96	−0.16 ± 0.02	0.67 ± 0.10
	σ_θ = 25.9–26.3	31.74°N,64.32°W	5.60 ± 1.41	-10.49 ± 4.21	198.67 ± 46.35	96.00 ± 24.42	−0.41 ± 0.01	0.80 ± 0.09
Bermuda 6976	25 m to 75 m	31.76°N,64.16°W	12.15 ± 3.45	-6.69 ± 1.74	199.00 ± 69.95	100.13 ± 15.47	1.69 ± 0.01	0.54 ± 0.08
	σ_θ = 25.4–25.9	31.76°N,64.16°W	10.69 ± 2.58	-18.09 ± 5.81	199.00 ± 84.79	151.00 ± 2.00	1.06 ± 0.04	0.63 ± 0.12
	σ_θ = 25.9–26.3	31.76°N,64.16°W	20.64 ± 11.44	-13.39 ± 1.82	176.00 ± 63.06	145.00 ± 38.46	1.31 ± 0.02	0.62 ± 0.08
Bermuda 6975	25 m to 75 m	31.61°N,64.22°W	15.61 ± 3.77	-5.71 ± 1.65	117.14 ± 20.15	102.33 ± 26.03	2.22 ± 0.03	0.51 ± 0.10
	σ_θ = 25.2–25.8	31.61°N,64.22°W	18.63 ± 14.98	-8.06 ± 4.11	107.25 ± 37.70	144.00 ± 44.67	−0.03 ± 0.05	0.38 ± 0.12
	σ_θ = 25.8–26.3	31.61°N,64.22°W	16.36 ± 8.49	-5.92 ± 1.07	99.00 ± 20.55	128.60 ± 30.34	0.06 ± 0.03	0.52 ± 0.10
Bermuda 7663	25 m to 75 m	31.73°N,64.20°W	5.74 ± 1.10	-7.06 ± 2.62	164.60 ± 28.47	109.00 ± 20.96	0.22 ± 0.01	0.72 ± 0.09
	σ_θ = 25.3–25.8	31.73°N,64.20°W	12.25 ± 4.16	-12.37 ± 3.99	102.60 ± 16.29	92.00 ± 15.14	−0.19 ± 0.02	0.65 ± 0.08
	σ_θ = 25.8–26.3	31.73°N,64.20°W	2.13 ± 0.99	-4.20 ± 1.27	83.00 ± 20.50	147.75 ± 26.58	−0.65 ± 0.01	0.31 ± 0.07

negative residual $PreNO_3$ anomalies were not observed outside of the latitudinal range between 40°S and 40°N (Fig. 2B). Float observed negative residual $PreNO_3$ within 100-150 m is concentrated within the central North Pacific in the vicinity of the Hawaiian islands and within the western Sargasso Sea of the North Atlantic in the vicinity of Bermuda (Fig. 2B). These two regions are selected for further analysis of the spatiotemporal patterns of residual $PreNO_3$ anomaly magnitudes and formation rates.

3.2. Hawaii and North Pacific residual $PreNO_3$ anomalies

The geographical float path of a typical BGC-Argo float deployment in the subtropical North Pacific near Hawaii (Float Hawaii 8486) with its observed NO_3, O_2, and calculated residual $PreNO_3$ and AOU tracers in

the upper 350 m is plotted in Fig. 3. For the upper 100 m (i.e. the approximate euphotic zone) there is a general seasonal cycle between negative residual $PreNO_3$ anomalies present in the winter and positive residual $PreNO_3$ anomalies for the rest of the year (Fig. 3B) that is similarly present in the other Hawaii float records (Fig. S1, S3, S5, S7, S9). AOU generally shows net photosynthesis (negative values) in the upper 100 m (Fig. 3C), with episodes of transitioning to net respiration (positive values) during the winter due to convective mixing with waters deeper than 100 m exhibiting positive AOU year-round (also present in Fig. S1, S3, S5, S7, S9). However the AOU record for float Hawaii 6403 had negative AOU values in the upper 100 m throughout its time series (Fig. S3). NO_3 is near zero within the upper 100 m (Fig. 3D) and increases with depth, with the nitracline (e.g. $NO_3 \geq 1$ μM) being located at a mean depth of 132 m throughout the Hawaii float records. Lastly, the mean O_2 concentration within the upper 100 m for the Hawaii floats is 192.91 μM and decreases with depth (Fig. 3, S1, S3, S5, S7, S9). All Hawaii and North Pacific profiling float records exhibited positive residual $PreNO_3$ anomalies ($PreNO_3 > 0$) in the upper ocean (<~100 m) and typically exhibited negative residual $PreNO_3$ anomalies ($PreNO_3 < 0$) at depths of ~100–250 m, however negative residual $PreNO_3$ anomalies were observed infrequently in the records from EQPACW 12788 and CalCurrent 7647 compared to the other profiling floats (Figs. 3, 5, S1, S3, S5, S7, S9, S11, S13, S15, S17, S18, S19, S20, S21, S22, S23, S24, S25, S26).

The seasonality of the core of positive and negative residual $PreNO_3$ anomalies for all Hawaii and Bermuda (described in Section 3.3) BGC-Argo floats were calculated by taking the seasonal average depth of where the magnitude of the observed $PreNO_3$ was either positive or negative (Fig. 4A, C). In the subtropical North Pacific, the negative residual $PreNO_3$ anomalous layer retreats below 100 m starting in July and then starts shoaling towards the surface again starting in November (Fig. 4A). The core of positive residual $PreNO_3$ anomalies appear around Hawaii beginning at about 53 m in January and shoal to approximately 51 m by May, followed by an increase in depth back to roughly 53 m by December (Fig. 4A). Whereas the core of negative residual $PreNO_3$ anomalies appear around Hawaii beginning at about 102 m in January and increase to roughly 150 m depth by July, followed by shoaling back to approximately 120 m by December (Fig. 4A). Near Hawaii, the seasonal core of negative AOU values at ~40–80 m (Fig. 4B) is located slightly deeper than the core of positive residual $PreNO_3$ anomalies at ~50–54 m (Fig. 4A).

3.3. Bermuda and North Atlantic residual $PreNO_3$ anomalies

The geographical float path of a typical BGC-Argo float deployment in the subtropical North Atlantic near Bermuda (Float Bermuda 7663) with its observed NO_3, O_2, and calculated residual $PreNO_3$ and AOU tracers in the upper 350 m is plotted in Fig. 5. A similar seasonal cycle between negative residual $PreNO_3$ anomalies in the winter and positive residual $PreNO_3$ anomalies for the rest of the year in the upper 100 m can be seen in the other Bermuda residual $PreNO_3$ records (Fig. S11, S13, S15). Additionally a similar trend can be seen in the Bermuda AOU records where AOU showed net photosynthesis (negative values) in the upper 100 m, with episodes of transitioning to net respiration (positive values) during the winter due to convective mixing (Fig. 5, S11, S13, S15). NO_3 is near zero with the upper 100 m (Fig. 5D) and increases with depth, with the nitracline (e.g. $NO_3 \geq 1$ μM) being located at a mean depth of 111 m throughout the Bermuda float records. Lastly, the mean O_2 concentration within the upper 100 m is 201.99 μM and decreases with depth (Fig. 5, S11, S13, S15). All Bermuda profiling float records had positive residual $PreNO_3$ anomalies ($PreNO_3 > 0$) in the upper ocean (<~100 m) and typically exhibited negative residual $PreNO_3$ anomalies ($PreNO_3 < 0$) at depths of ~100–250 m (Fig. 5, S11, S13, S15).

In the subtropical North Atlantic, the negative residual $PreNO_3$ anomalous layer retreats below 100 m starting in June and then begins shoaling towards the surface again starting in November (Fig. 4C). The core of positive residual $PreNO_3$ anomalies appear around Bermuda beginning at about 58 m in January and shoal to approximately 54 m by July, followed by an increase in depth to roughly 57 m by December (Fig. 4C). Whereas the core of negative residual $PreNO_3$ anomalies appear around Bermuda beginning at about 120 m in January and increase to roughly 150 m depth by June, followed by shoaling back to approximately 120 m by December (Fig. 4C). Near Bermuda, the seasonal core of negative AOU values present at ~30–60 m (Fig. 4D) generally tracks the core of positive residual $PreNO_3$ anomalies at ~51–59 m (Fig. 4C).

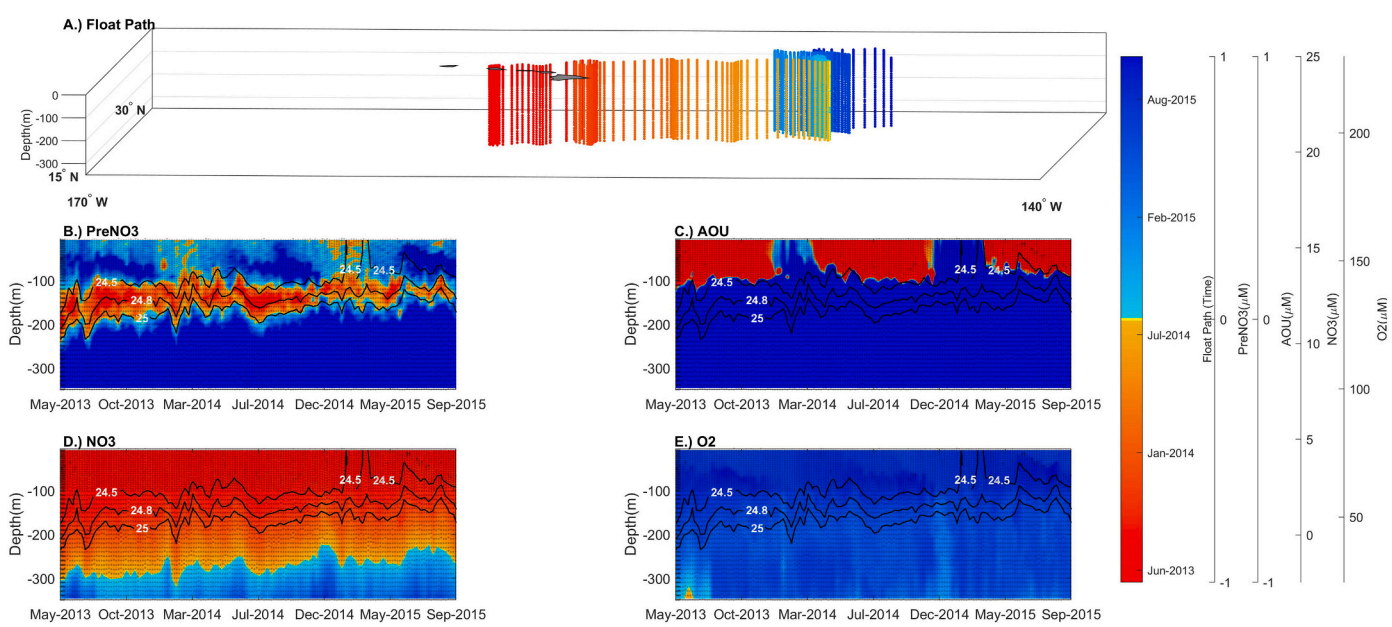

Fig. 3. A.) Float path of Hawaii 8486 colored by time. Residual $PreNO_3$ [μM] (B), AOU [μM] (C), NO_3 [μM] (D), and O_2 [μM] (E) for the first 350 m of the water column along the float path from May 2013 to Nov 2015. Black lines in B-E represent isopycnals, $\sigma_\theta = 24.5$, 24.8, and 25.0, chosen to outline anomalies. Dots in B-E represent observations. Residual $PreNO_3$ and AOU limited to a range of −1 to 1 μM to highlight negative (red) and positive (blue) values. (For interpretation of the references to colour in this figure legend, the reader is referred to the web version of this article.)

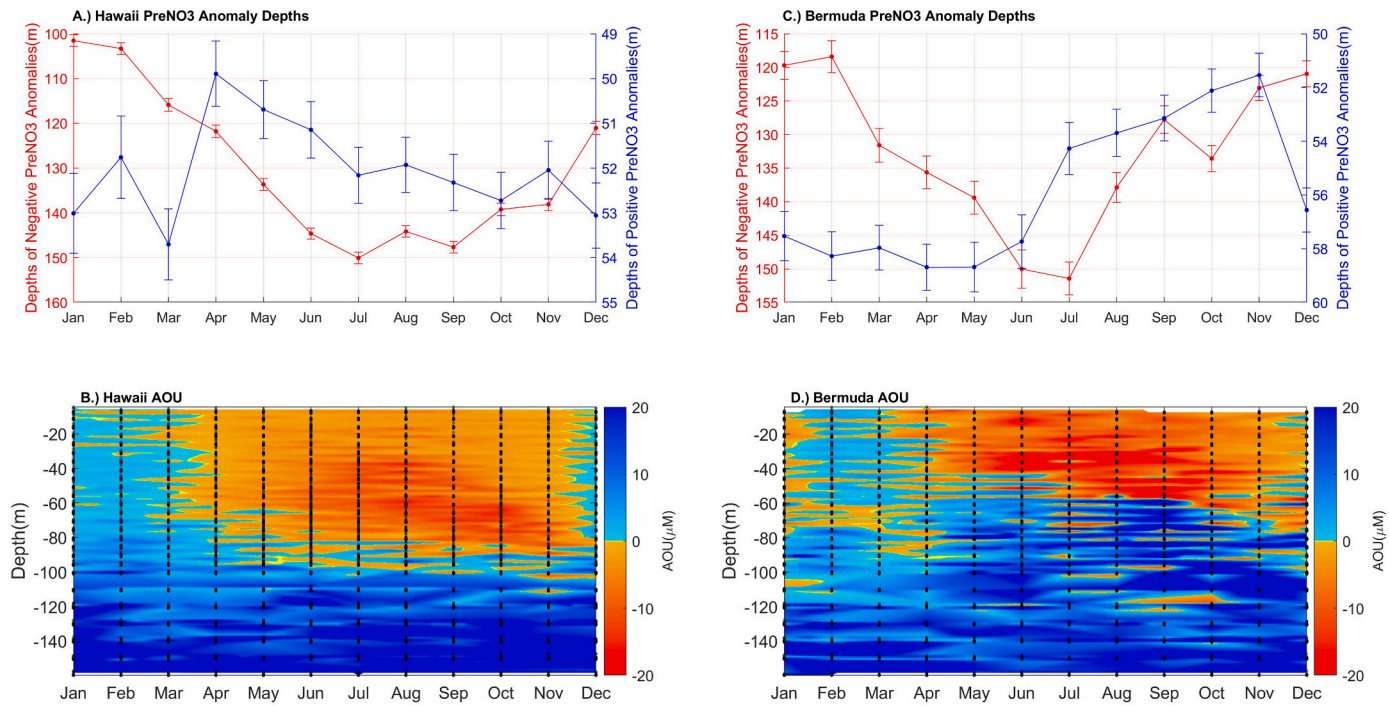

Fig. 4. Hawaii and Bermuda seasonal AOU and residual $PreNO_3$ anomaly depths. A.) Monthly depths for the core of subsurface negative $PreNO_3$ anomalies (red) and of euphotic zone positive residual $PreNO_3$ anomalies (blue) from Hawaii BGC-Argo floats. B.) Monthly AOU derived from Hawaii BGC-Argo float observations for 0-160 m. C.) Monthly depths for the core of subsurface negative residual $PreNO_3$ anomalies (red) and of euphotic zone positive residual $PreNO_3$ anomalies (blue) from Bermuda BGC-Argo floats. D.) Monthly AOU derived from Bermuda BGC-Argo float observations for 0-160 m. Black dots in B.) and D.) represent observations. (For interpretation of the references to colour in this figure legend, the reader is referred to the web version of this article.)

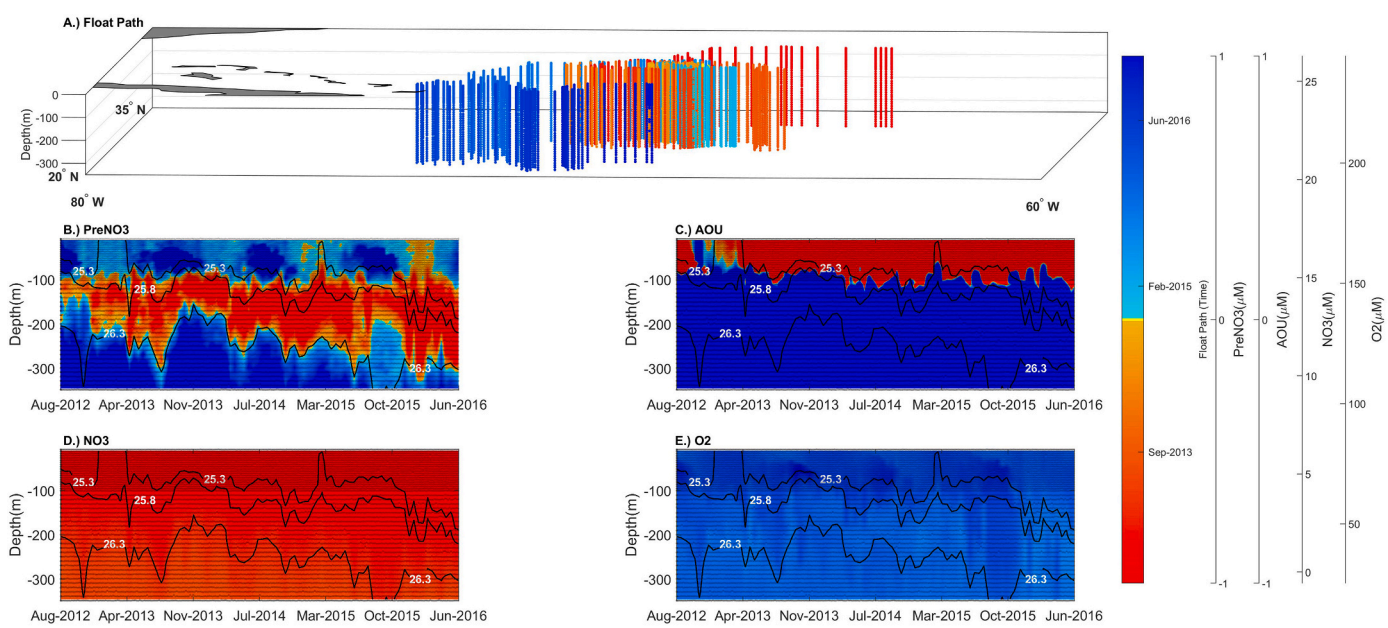

Fig. 5. A.) Float path of Bermuda 7663 colored by time. Residual $PreNO_3$ [μM] (B), AOU [μM] (C), NO_3 [μM] (D), and O_2 [μM] (E) for the first 350 m of the water column along the float path from Aug 2012 to Dec 2016. Black lines in B-E represent isopycnals $\sigma_\theta = 25.3$, 25.8, and 26.3, chosen to outline anomalies. Dots in B-E represent observations. Residual $PreNO_3$ and AOU limited to a range of −1 to 1 μM to highlight negative (red) and positive (blue) values. (For interpretation of the references to colour in this figure legend, the reader is referred to the web version of this article.)

3.4. Rates of residual $PreNO_3$ anomaly formation

Monthly to seasonal rates of residual $PreNO_3$ anomaly formation were estimated within three discrete depth/density layers for each of the twenty floats. Fig. 6 presents the residual $PreNO_3$ versus time record for floats Hawaii 8486 and Bermuda 7663 with the remaining presented in the Supplement, and summarized in Table 2. In the residual $PreNO_3$ record for Hawaii 8486 there were 5 positive and 3 negative trends observed within the 25-75 m depth layer ranging from 4.88 to −5.26 $\frac{\mu mol\ N}{m^3\ day}$, 4 positive and 3 negative trends within the $\sigma_\theta = 24.5$–24.8 density

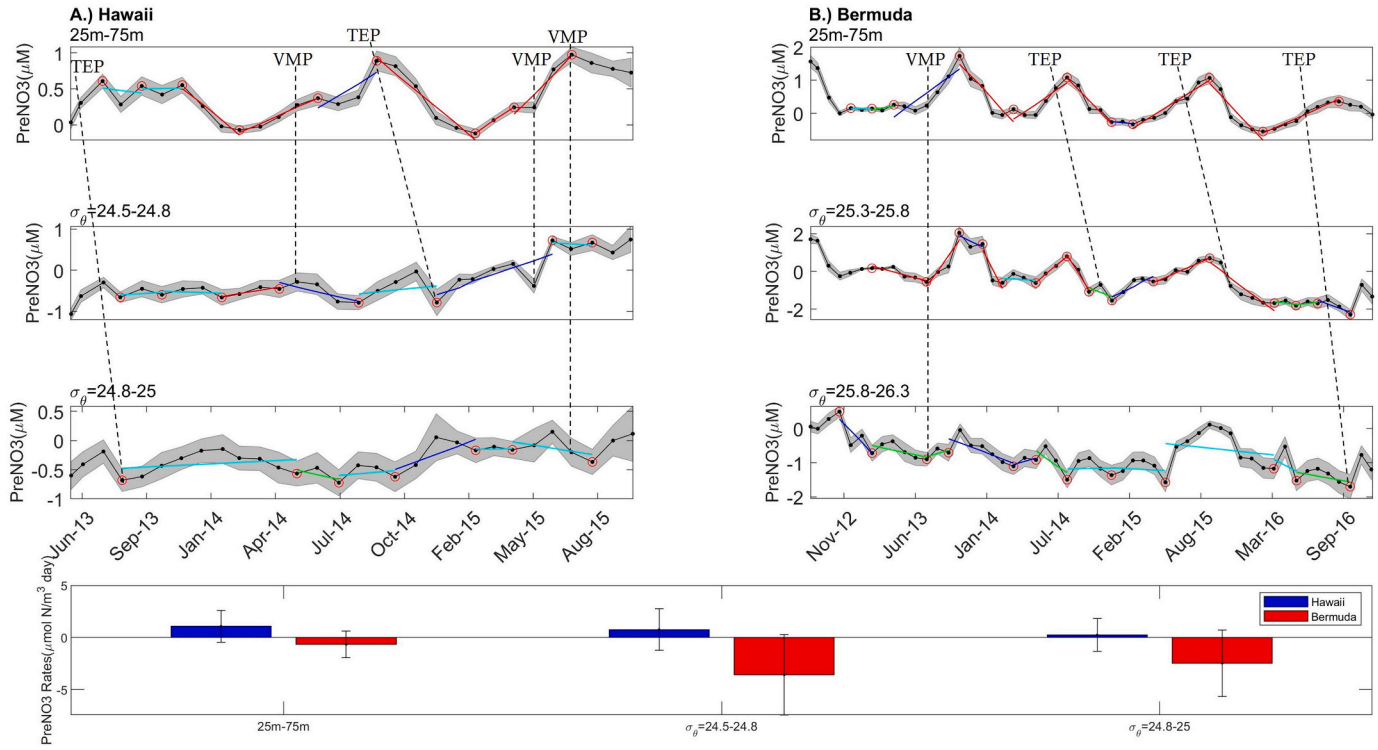

Fig. 6. A.) Residual $PreNO_3$ [μM] for Hawaii 8486 smoothed to show residual $PreNO_3$ per month with regression of residual $PreNO_3$ vs time. B.) Residual $PreNO_3$ [μM] as in A) for Bermuda 7663. Top panels are residual $PreNO_3$ at 25-75 m, middle panels are residual $PreNO_3$ at $\sigma_\theta = 24.5$–24.8 for Hawaii and $\sigma_\theta = 25.3$–25.8 for Bermuda, bottom panels are residual $PreNO_3$ at $\sigma_\theta = 24.8$–25.0 for Hawaii and $\sigma_\theta = 25.8$–26.3 density layer for Bermuda. Black dots are observations; red circles are local minima and maxima. Regressions are colored by the value of the correlation coefficient; $r^2>0.75$ (Red), $0.75> r^2>0.5$ (Blue), $0.5> r^2>0.25$ (Green), $0.25> r^2>0$ (Cyan). Grey regions represent 95% confidence intervals for residual $PreNO_3$ values. The dashed lines represent observations of TEP and VMP events between the three layers (discussed in Section 4.2). The bottom bar graph is a comparison of the rates of residual $PreNO_3$ anamoly formation between the two floats in each layer. (For interpretation of the references to colour in this figure legend, the reader is referred to the web version of this article.)

layer ranging from 2.64 to −1.74 $\frac{\mu mol\ N}{m^3\ day}$, and 4 positive trends and 2 negative trends within the $\sigma_\theta = 24.8$–25.0 density layer ranging from 1.46 to −2.17 $\frac{\mu mol\ N}{m^3\ day}$ (Fig. 6A). Although both positive and negative $PreNO_3$ anomaly formation rates were observed for each depth/density layer for each Hawaii float, $PreNO_3$ concentrations are overall positive for the 25-75 m layer (mean = −0.01 to 0.42 μM), and negative for the $\sigma_\theta = 24.5$–24.8 layer (mean = −0.92 to −0.07 μM), and $\sigma_\theta = 24.8$–25.0 density layer (mean = −0.67 to −0.29 μM) (Table 2). Net $PreNO_3$ anomaly formation rates are neutral to slightly positive for the three depth/density layers for Hawaii 8486 (Fig. 6). This pattern largely holds for the other five Hawaii floats with evidence of net negative formation rates for the subsurface density layers in some float records, e.g. Hawaii 5145 and Hawaii 6891 (Table 2). For the Hawaii floats the length of positive trends ranged from 81.9 ± 9.2 days to 187.4 ± 53.5 days, whereas the length of negative trends ranged from 61.3 ± 1.3 days to 180.0 ± 44.6 days (Table 2).

Similar $PreNO_3$ anomaly formation trends, magnitudes, and trend lengths were found for Bermuda 7663 and the other three Bermuda floats (Table 2). $PreNO_3$ anomaly formation rates were generally 4 to 10 times larger across depth/density layers for the Bermuda as compared to the Hawaii floats (Table 2). Trend lenghths were similar, ranging from 83.0 ± 20.5 to 199.0 ± 84.8 days for positive $PreNO_3$ anomaly formation events and 76.5 ± 7.0 to 151.0 ± 2.0 days for negative anomaly events. $PreNO_3$ concentrations were overall positive for the 25-75 m layer (mean = 0.17 to 2.22 μM), spanning positive, neutral, and negative for the $\sigma_\theta = 25.3$–25.8 layer (mean = −0.19 to 1.06 μM), and $\sigma_\theta = 25.8$–26.3 density layer (mean = −0.65 to 1.31 μM) (Table 2). However, net $PreNO_3$ anomaly formation rates are neutral for the euphotic zone and net negative for the subsurface density layers for Bermuda 7663 (Fig. 6). The pattern largely holds for the other Bermuda floats with some exhibiting closer to neutral net $PreNO_3$ anomaly formation rates in the subsurface layers (Table 2).

Based on the rates of residual $PreNO_3$ anomaly formation observed in the middle and bottom subsurface density layers from all six Hawaii and four Bermuda BGC-Argo float records, the middle subsurface density layer has a greater mean positive rate of $PreNO_3$ anomaly formation (7.82 $\frac{\mu mol\ N}{m^3\ day}$) than the bottom subsurface density layer (6.70 $\frac{\mu mol\ N}{m^3\ day}$) (Table 2). Additionally the middle subsurface density layer has a greater mean negative rate of $PreNO_3$ anomaly formation (−7.11 $\frac{\mu mol\ N}{m^3\ day}$) than the bottom subsurface density layer (−5.49 $\frac{\mu mol\ N}{m^3\ day}$) (Table 2). The rates of residual $PreNO_3$ anomaly formation reported for Station ALOHA from Letscher & Villareal, (2018) (negative rates ranging from −1.6 to −3.0 $\frac{\mu mol\ N}{m^3\ day}$ and positive rates ranging from 2.4 to 3.3 $\frac{\mu mol\ N}{m^3\ day}$) roughly agree with the rates seen in the Hawaii float records, however the rates observed for the Bermuda floats are ~2–3 times greater than those from Letscher & Villareal, (2018) from the BATS station (negative rates ranging from −3.8 to −5.5 $\frac{\mu mol\ N}{m^3\ day}$ and positive rates ranging from 4.1 to 5.8 $\frac{\mu mol\ N}{m^3\ day}$).

3.5. *Residual $PreNO_3$ anomaly seasonality*

All profiling floats in our analysis with the exception of EQPACW 12788 and CalCurrent 7647 exhibited both euphotic zone positive residual $PreNO_3$ anomalies (i.e. $[PreNO_3] > 0$) and subsurface negative residual $PreNO_3$ anomalies (i.e. $[PreNO_3] < 0$) on seasonal to perennial timescales along their float paths in the subtropical ocean (Figs. 3, 5, S1, S3, S5, S7, S9, S11, S13, S15, S17, S18, S19, S20, S21, S22, S23, S24,

S25, S26). The seasonality of residual $PreNO_3$ anomalies within the three discrete depth/density layers was examined by calculating monthly averages of the depths at which the 'core' of positive and negative residual $PreNO_3$ anomalies occurred for the BGC-Argo floats in Table 2 within two groups: 'Hawaii' and 'Bermuda'. For the Hawaii floats, residual $PreNO_3$ values increase in the spring and summer from values of ~0.10 μM to ~0.76 μM whereas they decrease from values of ~0.85 μM to ~0.01 μM in the winter and fall within 25-75 m (Fig. 7). Hawaii floats residual $PreNO_3$ values in the subsurface are constant during the winter at a value of ~ − 0.82 μM whereas they decrease from values of ~ − 0.39 μM to ~ − 0.83 μM during the spring, summer and fall (Fig. 7). For the Bermuda floats, residual $PreNO_3$ values increase in the winter from values of ~0.83 μM to ~1.11 μM and from ~1.14 μM to ~1.33 μM in the summer whereas they decrease in the fall from values of ~1.31 μM to ~0.58 μM and from ~1.44 μM to ~0.97 μM in the spring within 25-75 m (Fig. 7). Bermuda floats residual $PreNO_3$ values in the subsurface increase in the winter from values of ~0.17 μM to ~0.49 μM whereas they decrease in the summer from ~0.06 μM to ~ − 0.01 μM, in the fall from values of ~ − 0.16 μM to ~ − 0.19 μM and from ~ − 0.01 μM to ~ − 0.28 μM in the spring (Fig. 7).

4. Discussion

4.1. Patterns and rates of residual $PreNO_3$ anomalies across the Pacific and Atlantic oceans

Residual $PreNO_3$ derived from World Ocean Atlas 2018 data at 150 m (Fig. 2A) indicates that negative residual $PreNO_3$ anomalies occur primarily between 30°S and 30°N, which was the motivation for choosing BGC-Argo profiling floats that primarily transited between 40°S and 40°N (Fig. 2B). With exception of the profiling floats which did not have negative residual $PreNO_3$ anomalies in their records (EQPACW 12788 and CalCurrent 7647) euphotic zone positive residual $PreNO_3$ anomalies and subsurface negative residual $PreNO_3$ anomalies persist seasonally throughout the BGC-Argo residual $PreNO_3$ record (Figs. 2, 3, 5, S1, S3, S5, S7, S9, S11, S13, S15, S17, S18, S19, S20, S21, S22, S23, S24, S25, S26, S28, S29). Euphotic zone positive residual $PreNO_3$ anomalies generally follow a seasonal cycle in which residual $PreNO_3$ increases during the late spring to late fall, being replaced by negative values in winter (Figs. 3, 5, 6, 7). Subsurface negative residual $PreNO_3$ anomalies are generally perennial features throughout the subtropics (Figs. 2, 3, 5, 6). While there were BGC-Argo float records that showed negative residual $PreNO_3$ anomalies reaching deeper than 250 m, the majority of Pacific and Atlantic BGC-Argo floats exhibited subsurface negative residual $PreNO_3$ anomalies between 100 m and 250 m (Figs. 3, 5, S1, S3, S5, S7, S9, S11, S13, S15, S17, S18, S19, S20, S21, S22, S23, S24, S25, S26). The general observation of cycling between negative residual $PreNO_3$ anomalies in the winter and positive residual $PreNO_3$ anomalies for the rest of the year in the upper 100 m is likely due to winter vertical mixing redistributing the subsurface negative residual $PreNO_3$ anomaly signal (Figs. 3, 5, S1, S3, S5, S7, S9, S11, S13, S15, S17, S18, S19, S20, S21, S22, S23, S24, S25, S26). While the euphotic zone consistently exhibits positive residual $PreNO_3$ concentrations and the shallow subsurface consistently exhibit negative residual $PreNO_3$ concentrations for many of the BGC-Argo float records (Figs. 3, 5, S1, S3, S5, S7, S9, S11, S13, S15, S17, S18, S19, S20, S21, S22, S23, S24, S25, S26), each layer containing negative residual $PreNO_3$ concentrations can display both positive and negative changes in residual $PreNO_3$ concentrations, i.e. a $PreNO_3$ anomaly formation rate (Table 2). Ocean basin comparison of residual $PreNO_3$ anomaly formation rates show that the Hawaii floats most often exhibited the minimum positive or negative rates (i.e. smaller overall magnitudes) across the three depth/density layers, as compared to the Bermuda floats (Table 2; Section 3.3).

Focusing on the seasonality of residual $PreNO_3$ within the euphotic zone and shallow subsurface for the Hawaii and Bermuda floats, we find that both increasing residual $PreNO_3$ near the surface and decreasing residual $PreNO_3$ in the subsurface commence in May/June and progress through Oct/Nov with a dynamic range on the order of ~0.5–1 μM (Fig. 7). The Hawaii float averaged euphotic zone residual $PreNO_3$ is near a value of zero in winter, increasing to ~1 μM in September before

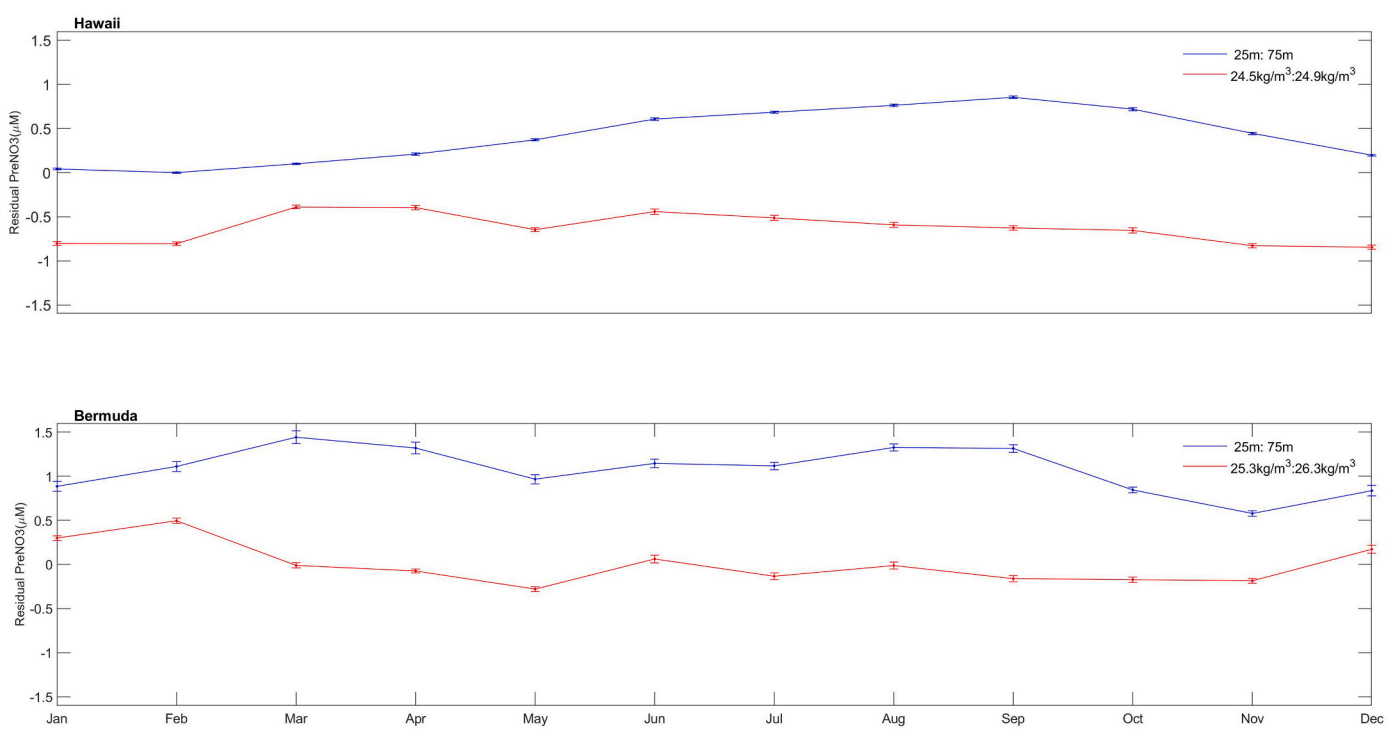

Fig. 7. Seasonality of residual $PreNO_3$ [μM] observations from the Hawaii and Bermuda floats. Blue lines are monthly averaged residual $PreNO_3$ within 25-75 m. Red lines are monthly averaged residual $PreNO_3$ within chosen isopycnals. (For interpretation of the references to colour in this figure legend, the reader is referred to the web version of this article.)

descreasing again (Fig. 7). Hawaii float averaged subsurface residual $PreNO_3$ is negative in value across months, with a maxima in Mar-Jun that is ~0.5 μM greater than the minima in Nov-Feb (Fig. 7). For the Bermuda averaged floats, euphotic zone residual $PreNO_3$ is positive in value year round with twin peaks in Feb-Apr and Aug/Sep that are ~0.5 μM greater than the minima in Nov/Dec (Fig. 7). Bermuda averaged subsurface residual $PreNO_3$ is positive in Dec-Feb before decreasing to values at or below zero for the remainder of the year. The monthly averaged depths of the core of the negative residual $PreNO_3$ anomaly layers appear to track the seasonal changes in the euphotic zone, since the depths of the core of the negative residual $PreNO_3$ anomaly layers descend ~30–50 m and are deepest in the summer and shallowest in winter for both the Hawaii and Bermuda floats (Fig. 4). This can also be seen in the seasonality of the distribution of negative residual $PreNO_3$ anomalies, where negative residual $PreNO_3$ anomalies generally descend below 100 m in summer and then ascend again in the winter (Fig. S28, S29). Seasonal variability for the depth of the core of positive residual $PreNO_3$ anomaly layers within the Hawaii and Bermuda floats is more muted, with a change of only a few meters (Fig. 4).

Based on the observed seasonal patterns, we speculate that whichever process(es) are responsible for driving residual $PreNO_3$ anomalies across the upper ocean of the subtropical North Pacific and North Atlantic might be linked to the well-documented unexplained summertime DIC drawdown from the surface mixed layer (e.g. Michaels et al., 1994; Keeling et al., 2004). For example, both the net community production resulting in the net production of TEP or that fueled by VMP should be expected to continue upwards vertically from the investeigated 25-75 m layer of our analysis into the surface mixed layer, with the observation of a $PreNO_3$ anomaly erased by the sea to air gas exchange of O_2. The near equivalence of the absolute value of euphotic zone positive rates of residual $PreNO_3$ anomaly formation compared to the absolute value of subsurface negative rates of residual $PreNO_3$ anomaly formation can speak to the potential linkage of the anomaly generating mechanism across depths. For the Hawaii and Bermuda floats, absolute values for euphotic zone positive rates of residual $PreNO_3$ anomaly formation are roughly equivalent to the absolute value of the negative rates within the subsurface layers. This suggests that whatever process(es) is causing anomalies in the euphotic zone may be related to the process(es) that is causing residual $PreNO_3$ anomalies in the subsurface layers in a mass balance sense. Although BGC-Argo floats approach a Lagrangian view of the ocean, the nine day park at 1000 m depth before performing a depth profile means that a float does not resurface in the same water parcel every ten days. Thus, caution should be used when interpreting potentially vertically connected processes and lateral gradients in residual $PreNO_3$ may also play a role in the temporal trends in residual $PreNO_3$ observed by a float.

4.2. Evidence for residual $PreNO_3$ anomaly generating mechanisms: vertically migrating phytoplankton and transparent exopolymer particles

With acknowledgement of the semi-Lagrangian sampling scheme of the BGC-Argo floats over their multi-year deployments, here we attempt to ascribe the temporal and vertical coupling of residual $PreNO_3$ anomaly formation patterns to one of two generating mechanisms: vertically migrating phytoplankton (VMP) or TEP cycling. Whether TEP or VMP is responsible for residual $PreNO_3$ anomalies can potentially be examined by comparing the timing of euphotic positive residual $PreNO_3$ anomaly formation events with the timing of sub-euphotic zone negative residual $PreNO_3$ anomaly formation events. Newly produced TEP is positively buoyant, and is only thought to attain negative buoyancy (sinking rate of order 10s meters per year) after aggregation and incorporation of ballasting material from the water column (Mari et al., 2017). Thus TEP contribution to positive and negative residual $PreNO_3$ anomaly formation should manifest as periods of net positive residual $PreNO_3$ anomaly formation within the euphotic zone leading by weeks to months, negative residual $PreNO_3$ anomaly formation within the shallow subsurface layers. This timescale allows for the biological production of TEP precursor carbohydrates and their abiotic aggregation as TEP (generating the positive residual $PreNO_3$ anomaly in the euphotic zone), followed by slow sinking of TEP to the shallow subsurface whereby it is respired, generating negative residual $PreNO_3$ anomalies as oxygen is consumed without a Redfieldian accumulation of nitrate (Fig. 1). By contrast, the contribution of VMP to euphotic zone positive and subsurface negative residual $PreNO_3$ anomaly formation is expected to be contemporaneous, since migrator ascent/descent velocities have been measured on the order of meters per hour with full migration cycles taking on the order of 3–6 days (Villareal et al., 1996).

Events of both TEP and VMP contribution to euphotic zone positive and subsurface layer negative residual $PreNO_3$ anomaly formation have been indentified for all Hawaii and Bermuda floats analyzed in this study (Fig. 6, S2, S4, S6, S8, S10, S12, S14, S16). For example, two residual $PreNO_3$ anomaly generating events from float Hawaii 8486 were identified during the spring to summer of 2010 and summer to early fall in 2011 potentially attributed to TEP (Fig. 6A). Increasing residual $PreNO_3$ concentrations within the 25-75 m layer precede decreasing residual $PreNO_3$ concentrations in the $\sigma_\theta = 24.25–24.75$ kg/m^3 density layer by ~3–4 months. A residual $PreNO_3$ anomaly generating event was observed by this same float in July 2013 attributed to VMP due to the contemporaneous increasing residual $PreNO_3$ within the 25-75 m layer and decreasing residual $PreNO_3$ within the density layer immediately below (Fig. 6A). Simarily, three residual $PreNO_3$ anomaly formation events were observed for float Bermuda 7663 attributed to TEP in mid-2014, 2015, and 2016 with an additional residual $PreNO_3$ anomaly generating event from July 2013 attributed to VMP (Fig. 6B).

When normalized to the number of float records for each region in our analysis, both the Hawaii and Bermuda floats exhibited evidence for a TEP event at a rate of ~2 per float record or approximately annually. VMP events near Hawaii were observed at a similar rate, while VMP events near Bermuda were observed at half that rate, ~1 per float record. Thus it seems that both VMP and TEP are equally important in causing the formation of residual $PreNO_3$ anomalies around Hawaii in the subtropical North Pacific, while TEP may be a more important contributor around Bermuda in the Sargasso Sea. Four out of the five BGC-Argo floats investigated in Fawcett et al. (2018) were also used for this research; Bermuda 7663, Bermuda 6391, Bermuda 6975, and Bermuda 6976 (Fig. 5, S11, S13, S15). Our estimates of the preponderance of TEP causing the formation of residual $PreNO_3$ anomalies from floats Bermuda 7663, Bermuda 6391, Bermuda 6975, and Bermuda 6976 agree with the suggestion by Fawcett et al. (2018) that the remineralization of TEP (referred to as gel-like organic matter by those authors) is an important process responsible for subsurface negative residual $PreNO_3$ anomaly formation (Fig. 6B, S12, S14, S16) in the Sargasso Sea. However, putative VMP events were still observed in the residual $PreNO_3$ records of floats Bermuda 7663, Bermuda 6391, and Bermuda 6975 (Fig. 6B, S12, S14). The suggestion of a more important contribution for TEP to residual $PreNO_3$ anomaly formation in the Sargasso Sea as suggested by the BGC-Argo float record is at odds with that estimated at the BATS site in which VMP was estimated to account for >90% of the residual $PreNO_3$ anomalies (Letscher and Villareal, 2018). This estimate was based on very limited information regarding TEP concentrations and vertical gradients in the Sargasso Sea and should be followed up with new observational studies of both TEP concentrations and VMP biomass to resolve which mechanism is responsible for residual $PreNO_3$ anomaly formation in the Sargasso Sea. Hawaii 5145 is the same float that was examined in Johnson et al. (2010) and the estimate of one VMP event in the residual $PreNO_3$ records of Hawaii 5145 in our analysis (Fig. S2) agrees with the Johnson et al. (2010) suggestion that VMP is a potentially important mechanism for $PreNO_3$ anomaly formation in the subtropical North Pacific. The BGC-Argo record suggests VMP may be an equal contributor to residual $PreNO_3$ anomaly formation near Hawaii, in agreement with that suggested for Station ALOHA (Letscher and Villareal, 2018). We note observations of the presence of

known VMP taxa (e.g., *Pyrocystis, Ethmodiscus, Rhizosolenia*) are more frequent in the Pacific Ocean than the Atlantic Ocean (Letscher and Villareal, 2018).

To further explore the comparative importance of VMP and TEP mechanisms between the North Pacific and North Atlantic, we examined the spatiotemporal patterns of seasonal AOU and PreNO3 concentrations in the upper ocean (Fig. 4). Co-location in time and space of changes in AOU with that of residual $PreNO_3$ anomalies may provide insight as to the likelihood of the VMP mechanism since their photosynthesis should create a signal of negative AOU and positive and increasing residual $PreNO_3$ in the euphotic zone. Near Bermuda, the core of the negative AOU signal descends from ~30–40 m in May/June towards ~40–60 m in July to October while the core of the positive residual $PreNO_3$ anomalies is centered on 55 ± 5 m year-round (Fig. 4). Near Hawaii, the core of the negative AOU signal is found deeper at ~60–80 m in summer while the core of the positive residual $PreNO_3$ anomalies is located at 52 ± 2 m (Fig. 4). Co-location of these signals in depth and time near Bermuda is suggestive of a larger role for VMP since their metabolic and migratory patterns cause contemporaneous and stoichiometrically linked changes to the oxygen and nitrate pools across the upper ocean. The observation that these changes in AOU and positive residual $PreNO_3$ in the euphotic zone near Hawaii are separated by a few tens of meters in depth (Fig. 4) is suggestive that something else besides VMP could be causing euphotic zone positive $PreNO_3$ anomalies there, i.e. TEP.

5. Conclusions

Solving the mystery of the biogeochemical processes responsible for the generation of upper ocean residual $PreNO_3$ anomalies that oceanographers have been investigating for decades will give insight into the non-Redfield processes that account for changes in oxygen without Redfielian stoichiometric changes in nitrate. Additionally, the biogeochemical processes generating residual $PreNO_3$ anomalies across the euphotic and shallow subeuphotic zones of the ocean subtropics may be linked to the well-documented conundrum of summertime drawdown of mixed layer dissolved inorganic carbon in the absence of sufficient new nutrient fluxes (Fig. 1; Michaels et al., 1994; Toggweiler, 1994; Gruber et al., 1998; Keeling et al., 2004). BGC-Argo floats provide the opportunity to obtain high resolution observations of biogeochemical processes which can help find answers to many oceanographic questions such as what mechanisms may drive the formation of residual $PreNO_3$ anomalies. Analyses have shown that both euphotic zone positive and subsurface negative residual $PreNO_3$ anomalies are widespread in the subtropical ocean and while there is some variability in the residual $PreNO_3$ values and sign, these vertically segregated residual $PreNO_3$ anomalies are persistent seasonally recurring features in the BGC-Argo O_2 and NO_3 records. However due to the amount of time BGC-Argo floats spend at 1000 m depth (~9.5 days) there could be significant spatial differences between the water parcels that BGC-Argo floats sample on successive descent/ascent cycles (Claustre et al., 2019). Thus, the data records, residual $PreNO_3$ anomalies, and attributed generating mechanism (TEP vs. VMP) presented in our study do not reflect truly 1-D (vertical) processes. The geographic 'footprint' of the water masses that the BGC-Argo floats observe may be on the order of a few to 10's of km between successive profiles at a 10 day frequency. Temporal and spatial mapping of BGC-Argo vertical profiles to contemporaneous sea surface satellite observables such as sea surface height, chlorophyll, temperature, etc. may be one manner in which to address the hydrographic and biogeochemical variability of the water masses the BGC-Argo float encounters over its deployment, for example to identify the passing of a mesoscale eddy.

The observation of widespread residual $PreNO_3$ anomalies in the subtropical ocean suggests that the current class of Earth System Models (e.g. Moore et al., 2018; Stock et al., 2020), ocean colour based models (e.g. Westberry et al.2008; Silsbe et al., 2016), and particle flux models (e.g. DeVries et al., 2014; Cael and Bisson, 2018), are missing important non-Redfield processes that could exert a strong influence on the predicted strength of the biological pump. The locations of residual $PreNO_3$ anomalies are consistent with previous observations of VMP taxa (e.g. *Pyrocystis, Ethmodiscus, Rhizosolenia*) throughout the global subtropical ocean (Letscher and Villareal, 2018). The timing of euphotic zone positive residual $PreNO_3$ anomaly formation events in relation to subeuphotic zone negative residual $PreNO_3$ anomaly formation events suggests that both the export and remineralization of TEP as well as the utilization of nutracline nitrate stocks by VMP play roles in the formation of residual $PreNO_3$ anomalies. Our analysis cannot provide definitive conclusions as to which mechanism dominates but suggests possible preponderance of VMP operating in the North Pacific and TEP processes operating in the North Atlantic. We stress that further investigation is needed of both TEP and VMP abundance and associated $C:N:O_2$ stoichiometry to better understand the relative importance each mechanism imparts to the formation of residual $PreNO_3$ anomalies across space and time in the subtropical ocean. A preponderance of one residual $PreNO_3$ anomaly generating process, TEP vs. VMP, either regionally or globally across the subtropics could have an important impact on the biological pump and its sensitivity to climate change forcings. Because diatoms and other VMP taxa produce mineral ballasted organic matter and play an important role in global carbon export, the predicted expansion of the subtropical marine biome and its resident VMP over the 21st century could help buffer against any potential declines in the ocean's biological carbon pump. Conversely, if residual $PreNO_3$ anomaly formation is dominated by the TEP mechanism, this process likely acts as a positive feedback to the currently warming carbon climate system as expanding subtropical waters harboring inefficient carbon export by slowing sinking TEP replace mesotrophic marine biomes containing higher proportions of marine phytoplankton that produce ballasted organic matter. Identifying the globally or regionally dominant formation mechanism for subtropical ocean residual $PreNO_3$ anomalies and the related summertime mixed layer dissolved inorganic carbon drawdown remain important unresolved questions of ocean biogeochemistry.

Acknowledgments, samples, and data

These data were collected and made freely available by the International Argo Program and the national programs that contribute to it. (http://www.argo.ucsd.edu, http://argo.jcommops.org). The Argo Program is part of the Global Ocean Observing System. Argo (2000). Argo float data and metadata from Global Data Assembly Centre (Argo GDAC). SEANOE. http://doi.org/10.17882/42182

R.T.L acknowledges support from NSF OCE-1923687.

Data availability

The data used in this paper is publicly and freely available at [https://www.mbari.org/data/ocean-float-data/].

Appendix A. Supplementary data

Supplementary data to this article can be found online at https://doi.org/10.1016/j.marchem.2023.104248.

References

Abell, Jeffrey, Emerson, Steve, Keil, Richard G., 2005. Using preformed nitrate to infer decadal changes in DOM remineralization in the subtropical North Pacific. Glob. Biogeochem. Cycles 19. https://doi.org/10.1029/2004GB002285.

Alldredge, Alice L., Passow, Uta, Logan, Bruce E., 1993. The abundance and significance of a class of large, transparent organic particles in the ocean. Deep-Sea Res. I 40, 1131–1140.

Ballek, Robert W., Swift, Elijah, 1986. Nutrient-and light-mediated buoyancy control of the oceanic non-motile dinoflagellate *Pyrocystris notiluca* Murray *ex* Haeckel (1890). J. Exp. Mar. Biol. Ecol. 101, 175–192. https://doi.org/10.1016/0022-0981(86)90048-1.

Broecker, Wallace S., 1974. "No", a conservative water-mass tracer*. Earth Planet. Sci. Lett. 23, 100–107.
Busch, Kathrin, Endres, Sonja, Iversen, Morten H., Michels, Jan, Nothig, Eva-Maria, Engel, Anja, 2017. Bacterial colonization and vertical distribution of marine gel particles (TEP and CSP) in the Arctic Fram Strait. Front. Mar. Sci. 4 https://doi.org/10.3389/fmars.2017.00166.
Cael, B.B., Bisson, Kelsey, 2018. Particle flux parameterizations: quantitative and mechanistic similarities and differences. Front. Mar. Sci. 5 https://doi.org/10.3389/fmars.2018.00395.
Cisternas-Novoa, Carolina, Lee, Cindy, Engel, Anja, 2015. Transparent exopolymer particles (TEP) and Coomassie stainable particles (CSP): differences between their origin and vertical distributions in the ocean. Mar. Chem. 175, 56–71.
Claustre, Herve, Johnson, Kenneth S., Takeshita, Yuichiro, 2019. Observing the Global Ocean with biogeochemical-Argo. Annu. Rev. Mar. Sci. 12, 23–48. https://doi.org/10.1146/annurev-marine-010419-010956.
DeVries, Tim, Deutsch, Curtis, 2014. Large-scale variations in the stoichiometry of marine organic matter respiration. Nat. Geosci. 7 (12), 890–894.
DeVries, T., Liang, J.-H., Deutsch, C., 2014. A mechanistic particle flux model applied to the oceanic phosphorus cycle. Biogeosciences 11, 5381–5398. https://doi.org/10.5194/bg-11-5381-2014.
Emerson, Steven, Hayward, Thomas L., 1995. Chemical tracers of biological processes in shallow waters of North Pacific: preformed nitrate distributions. J. Mar. Res. 53, 499–513.
Engel, Anja, 2003. Distribution of transparent exopolymer particles (TEP) in the Northeast Atlantic Ocean and their potential significance for aggregation processes. Deep Sea Res. Part I 51, 83–92. https://doi.org/10.1016/j.dsr.2003.09.001.
Engel, Anja, Passow, Uta, 2001. Carbon and nitrogen content of transparent exopolymer particles (TEP) in relation to their Alcian blue adsorption. Mar. Ecol. Prog. Ser. 219, 1–10.
Fawcett, Sarah E., Johnson, Kenneth S., Riser, Stephen C., Van Oostende, Nicolas, Sigman, Daniel M., 2018. Low-nutrient organic matter in the Sargasso Sea thermocline: a hypothesis for its role, identity, and carbon cycle implications. Mar. Chem. https://doi.org/10.1016/j.marchem.2018.10.008.
Garcia, H.E., Weathers, K., Paver, C.R., Smolyar, I., Boyer, T.P., Locarnini, R.A., Zweng, M.M., Mishonov, A.V., Baranova, O.K., Seidov, D., Reagan, J.R., 2018a. World Ocean atlas 2018, volume 3: dissolved oxygen, apparent oxygen utilization, and oxygen saturation. In: Mishonov, A., Technical (Eds.), NOAA Atlas NESDIS, 83, p. 38.
Garcia, H.E., Weathers, K., Paver, C.R., Smolyar, I., Boyer, T.P., Locarnini, R.A., Zweng, M.M., Mishonov, A.V., Baranova, O.K., Seidov, D., Reagan, J.R., 2018b. World Ocean atlas 2018, volume 4: dissolved inorganic nutrients (phosphate, nitrate and nitrate+nitrite, silicate). In: Mishonov, A., Technical (Eds.), NOAA Atlas NESDIS, 84, p. 35.
Gruber, Nicolas, 2008. The marine nitrogen cycle: overview and challenges. Nitrogen Marine Environ. II, 1–50.
Gruber, N., Keeling, C.D., Stocker, T.F., 1998. Carbon-13 constraints on the seasonal inorganic carbon budget at the BATS site in the northwestern Sargasso Sea. Deep-Sea Res. I Oceanogr. Res. Pap. 45 (4–5), 673–717.
Johnson, Kenneth S., Riser, Stephen C., Karl, David M., 2010. Nitrate supply from deep to near-surface water of the North Pacific subtropical gyre. Nat. Lett. 465, 1062–1065.
Keeling, C.D., Brix, H., Gruber, N., 2004. Seasonal and long-term dynamics of the upper ocean carbon cycle at station ALOHA near Hawaii. Glob. Biogeochem. Cycles 18 (4).
Letscher, Robert T., Moore, J. Keith, 2015. Preferential remineralization of dissolved organic phosphorus and non-Redfield DOM dynamics in the global ocean: Impacts on marine productivity, nitrogen fixation, and carbon export. Glob. Biogeochem. Cycles 29 (3), 325–340.
Letscher, Robert T., Villareal, Tracey A., 2018. Evaluation of the seasonal formation of subsurface negative preformed nitrate anomalies in the subtropical North Pacific and North Atlantic. Biogeosciences 15, 6461–6480.
Mari, Xavier, Passsow, Uta, Migon, Christophe, Burd, Adrian B., Legendre, Louis, 2017. Transparent exopolymer particles: Effects on carbon cycling in the ocean. Prog. Oceanogr. 151, 13–37. https://doi.org/10.1016/j.pocean.2016.11.002.
Martiny, Adam C., Pham, C.T., Primeau, Francois W., Vrugt, Jasper A., Moore, J. Keith, Levin, Simon A., Lomas, Michael W., 2013. Strong latitudinal patterns in the elemental ratios of marine plankton and organic matter. Nat. Geosci. 6 (4), 279–283.
MBARI, 2017. FloatViz 6.0 - Apex/ISUS Data Visualization, mbari.org. https://www.mbari.org/science/upper-ocean-systems/chemical-sensor-group/floatviz/.
Michaels, A.F., Bates, N.R., Buesseler, K.O., Carlson, C.A., Knap, A.H., 1994. Carbon-cycle imbalances in the Sargasso Sea. Nature 372 (6506), 537–540.
Moore, Keith J., Weiwei, Fu, Primeau, Francois, Britten, Gregory L., Lindsay, Keith, Long, Matthew, Doney, Scott C., Mahowald, Natalie, Hoffman, Forrest, Randerson, James T., 2018. Sustained climate warming drives declining marine biological productivity. Science 359, 1139–1143.
Myklestad, Sverre M., 1995. Release of extracellular products by phytoplankton with special emphasis on polysaccharides. Sci. Total Environ. 165, 155–164.
Paulmier, A., Kriest, I., Oschlies, A., 2009. Stoichiometries of remineralisation and denitrification in global biogeochemical ocean models. Biogeosciences 6, 923–935.
Peltzer, Edward T., 2007. Matlab Scripts for Oceanographic Calculations: aou. Monterey Bay Aquarium Research Institute (MBARI).
Pilskaln, C.H., Villareal, T.A., Dennet, M., Darjangelo-Wood, C., Meadows, G., 2005. High concentrations of marine snow and diatom algal mats in the North Pacific Subtropical Gyre: implications for carbon and nitrogen cycles in the oligotrophic ocean. Deep Sea Res. Part I 52, 2315–2332.
Polovina, Jeffery J., Dunne, John P., Woodworth, Phoebe A., Howell, Evan A., 2011. Projected expansion of the subtropical biome and contraction of the temperate and equatorial upwelling biomes in the North Pacific under global warming. ICES J. Mar. Sci. https://doi.org/10.1093/icesjms/fsq198.
Redfield, A.C., Ketchum, B.H., Richards, F.A., 1963. The influence of organisms on the composition of sea water. The Sea 26–77.
Rivkin, Richard B., Swift, Elijah, Biggley, William H., Voytek, Mary A., 1984. Growth and carbon uptake by natural populations of oceanic dinoflagellates *Pyrocystis noctiluca* and *Pyrocystis fusiformis*. Deep Sea Res. Part A. 31, 353–367. https://doi.org/10.1016/0198-0149(84)90089-X.
Silsbe, Greg M., Behrenfeld, Michael J., Halsey, Kimberly H., Milligan, Allen J., Westberry, Toby K., 2016. The CAFE model: a net production model for global ocean phytoplankton. Glob. Biogeochem. Cycles 30, 1756–1777. https://doi.org/10.1002/2016GB005521.
Stock, Charles A., Dunne, John P., Fan, Songmiao, Ginoux, Paul, John, Jasmin, Krasting, John P., Laaufkotter, Charlotte, Paulot, Fabien, Zadeh, Niki, 2020. Ocean biogeochemistry in GFDL's earth system Model 4.1 and its response to increasing atmospheric CO_2. J. Adv. Model. Earth Syst. https://doi.org/10.1029/2019MS002043.
Sukhanova, I.N., Rudyakov, Y.A., 1973. Population composition and vertical distribution of *Pyrocystis pseudonoctiluca* (W. Thomson) in the western equatorial Pacific. In: Vinogradov, M.E. (Ed.), Life Activities of Pelagic Communities in the Ocean. Israeli Program Scientific Translation, pp. 218–228.
Teng, Yi-Cheng, Primeau, Francois W., Moore, J. Keith, Lomas, Michael W., Martiny, Adam C., 2014. Global-scale variations of the ratios of carbon to phosphorus in exported marine organic matter. Nat. Geosci. 7 (12), 895–898.
The MathWorks™, Inc, 2019. MATLAB R2019b. Natick, Massachusetts, United States.
Toggweiler, J.R., 1994. Vanishing in Bermuda. Nature 372 (6506), 505–506.
Villareal, Tracy A., Carpenter, Edward J., 1994. Chemical composition and photosynthetic characteristics of *Ethmodiscus Rex* (Bacillariophyceae): evidence for vertical migration. J. Phycol. 30, 1–8. https://doi.org/10.1111/j.0022-3646.1994.00001.x.
Villareal, Tracy A., Lipschultz, F., 1995. Internal nitrate concentrations in single cells of large phytoplankton from the Sargasso Sea. J. Phycol. 31, 689–696. https://doi.org/10.1111/j.0022-3646.1995.00689.x.
Villareal, Tracy A., Woods, Samantha, Moore, J. Keith, Culver-Rymsza, Karen, 1996. Vertical Migration of *Rhizosolenia* mats and their significance to NO_3^- fluxes in the central North Pacific gyre. J. Plankton Res. 18, 1103–1121.
Villareal, Tracy A., Joseph, Leanne, Brzezinski, Mark A., Shipe, Rebecca F., Lipschultz, Fredric, Altabet, Mark A., 1999. Biological and chemical characteristics of the Giant Diatom Ethmodiscus (Bacillariophyceae) in the Central North Pacific Gyre. J. Phycol. 35, 896–902. https://doi.org/10.1046/j.1529-8817.1999.3550896.x.
Villareal, Tracy A., Pilskaln, Cynthia H., Montoya, Joseph P., Dennett, Mark, 2014. Upward nitrate transport by phytoplankton in oceanic waters: balancing nutrient budgets in oligotrophic seas. PeerJ. https://doi.org/10.7717/peerj.302.
Wurl, Oliver, Miller, Lisa, Vagle, Svein, 2011. Production and fate of transparent exopolymer particles in the ocean. J. Geophys. Res. 116.